



Contents lists available at ScienceDirect

Journal of King Saud University – Science

journal homepage: www.sciencedirect.com

Original article

Structural and optical properties of transition metal ion-doped ordered mesoporous TiO₂ prepared by chelating-assisted evaporation induced self-assembly method

Bedor S. Alyahya

Department of Physics, Al Badayea College of Sciences and Arts, Qassim University, P.O. 64, Buraidah 51452, Saudi Arabia

ARTICLE INFO

Article history:

Received 7 March 2021

Revised 4 May 2021

Accepted 5 May 2021

Available online 11 May 2021

Keywords:

Mesoporous

Titanium dioxide

Transition metal oxide

Electrocatalysis

Self-assembly

ABSTRACT

This paper demonstrates the fabrication of highly ordered mesoporous titanium dioxide (OMT) with different transition metals (TM: Fe, Mn, and Ni) by employing a self-assembly surfactant template route. The ordered TM-loaded mesoporous TiO₂ (TM-OMT) has uniform mesopores (3–5 nm pore diameter), and a crystalline framework is successfully prepared via soft template strategy by employing Pluronic® F127 triblock copolymer as a chelating and structural directing agent. The structural and optical characteristics of the TM-OMT hybrids have been examined by scanning electron microscopy (SEM), transmission electron microscope (TEM), XRD, N₂-sorption isotherms, UV/visible diffuse reflectance spectroscopy, and X-ray photoelectron spectroscopy (XPS) reveals the successful incorporation of TM ions over the highly ordered mesostructured OMT. The XRD pattern evidenced that the obtained TM-doped OMT samples are pure anatase of the crystalline phase. By employing TEM analysis, the average particle size is estimated to be 2–2.7 nm, whereas diffraction patterns have evidenced the polycrystalline features of the mesoporous structure. The bandgap energy of TM-doped mesoporous decreases according to the particular metal and its amount due to the reduced particle size. This cost-effective method provides the exceptional potential to tune the optical features for TM-doped mesoporous TiO₂ materials for its optoelectronic applications and show more significant promise for energy conversion technologies.

© 2021 The Author(s). Published by Elsevier B.V. on behalf of King Saud University. This is an open access article under the CC BY license (<http://creativecommons.org/licenses/by/4.0/>).

1. Introduction

The energy crisis has been a global concern today, and the advancement and exploitation of innovative energy sources represented by solar energy and hydrogen energy are impending. Since the discovery by Fujishima & Honda using rutile titanium dioxide (TiO₂) materials for the H₂ generation from photocatalytic water splitting (Fujishima and Honda, 1972). TiO₂ is recognized as the most widely used material and a favorable candidate for dye-sensitized solar cells (DSSCs), polymer solar cells, heterojunctions-based solar cells, and photocatalytic applications (Fujishima et al., 2000). Particularly, DSSCs are a promising field of material sciences research due to their easy manufacturing,

cost-effectiveness, and good photo-conversion efficiency (Li and Liu, 2010). More importantly, mesoporous TiO₂ has received considerable recognition due to its great surface area (Calleja et al., 2004) and porosity (Zukalova et al., 2005). The high efficacy nano-structured cells such as DSSCs (Ahmad et al., 2017), hybrid SCs (Even et al., 2013), quantum dot SCs (Nozik, 2002) and hypro-organic plumage halide perovskites (PSCs) (Chung et al., 2016) have been produced by this structural framework.

Ordered mesoporous metal oxides tend to possess outstanding properties, ranging from an unusually high surface area, an easily adjustable pore size, high porosity, and large pore volume (Wagner et al., 2013). Mesoporous-templated TiO₂ materials were first published by Antonelli et al. in 1995 (Antonelli and Ying, 1995). Afterward, several routes have been employed to manufacture mesoporous TiO₂ with different mesophase structures such as 2D hexagonal, 3D cubic, and lamellar structure, involving sol-gel, solvothermal, sonochemical and hydrothermal approaches (Yu et al., 2007; Wang et al., 2004). Particularly, Soft-template methods of evaporation-induced self-assembly (EISA) methods built on amphiphilic block copolymers are effective and beneficial to fabricate mesoporous materials with different morphological features

E-mail addresses: bs.alyahya@qu.edu.sa, bedoryeha2021@gmail.com

Peer review under responsibility of King Saud University.



Production and hosting by Elsevier

<https://doi.org/10.1016/j.jksus.2021.101469>

1018-3647/© 2021 The Author(s). Published by Elsevier B.V. on behalf of King Saud University.

This is an open access article under the CC BY license (<http://creativecommons.org/licenses/by/4.0/>).

and tunable pore constructions and have the potential to apply on the commercial scale (Jo et al., 2013).

The metal doping in TiO₂ materials helps the visible wavelength's intrinsic features with enhanced photoresponse (Xie et al., 2013; Liu et al., 2013). Numerous research works have been dedicated to metal doping over the past decades over mesoporous TiO₂ (Reda et al., 2020; Khojasteh et al., 2016). Particularly, Ye et al. successfully fabricated the cobalt-doped mesoporous TiO₂ materials via the EISA process, resulting in an enhanced optical feature (Wang et al., 2015). Also, Li et al. (Li et al., 2017) have developed Co-doped ordered mesoporous TiO₂ for sensor applications using the EISA process. Earlier studies demonstrated that organic and inorganic species' co-assembly can be well-governed by applying ligands such as acetylacetone and acetic acid (Wang et al., 2015; Li et al., 2017). Enlightened by these research works, we used a soft-templating route to fabricate the highly ordered and crystalline (Fe, Ni, and Mn) doped mesoporous TiO₂ by employing tetra butyl titanate as Ti precursor and the pluronic F127 as the template. We use acetic acid as a chelating agent through the EISA method to regulate the hydrolysis and condensation of TiO₂ precursor by steadying the hydrolyzed Ti nanoentities through the chelation process. The optical, structural and morphological characterization of the obtained samples have been elucidated in detail.

2. Experimental details

2.1. Materials

Non-ionic surfactant Pluronic F127 (Mw = 12600, PEO₁₀₆PPO₇₀-PEO₁₀₆) and Titanium n-butoxide (Ti(OBu)₄, 99%) were obtained from Aldrich Corp.

2.2. Synthesis of TM doped TiO₂ mesoporous

The crystalline ordered TM-doped TiO₂ mesoporous were obtained by chelating assisted EISA method in an ethanolic/Pluronic F127/HCl/acetic acid (HOAc)/Ti(OBu)₄ mixed solution mixed through the template-carbonization approach. Typically, 2.0 g of pluronic F127 was dispersed in 20 ml of anhydrous ethanol and 2.4 g of conc. HCl (37%). Afterward, the obtained mixture was stirred continuously to create a transparent solution. Sequentially, 3.4 g of Ti(OBu)₄ and 2.4 g of acetic acid was introduced with a constant stirring process to attain a homogeneous greenish-yellow solution and then transported to Petri dishes. It was then subjected to solidifying materials at 100 °C for 24 h to eradicate the solvents. The obtained green film was then annealed with a ramping rate of 1 °C min⁻¹ to 350 °C in N₂ and detained for 3 h, subsequent in the carbon-supported amorphous TM-doped TiO₂ powders. Finally, the supported-carbon was removed and obtained TiO₂ powder crystallization acquired through successive heat treatment with a ramp rate of 1 °C min⁻¹ to 400 °C in the air for 3 h. The obtained products were assigned as M (x)-OMT, where M refers to the doping metal and x corresponding to the molar ratios of M/Ti in the synthetic process.

2.3. Material characterizations

XRD patterns were logged with a Bruker-Advance D8 instrument. The optical absorption spectra of materials were analyzed via spectrophotometer (Shimadzu UV-2600). TEM photographs were performed with a JEM- 2100F microscope (Japan). Nitrogen sorption isotherms were assessed via a NOVA 2200e analyzer. The specific surface areas of the mesoporous TiO₂ materials were estimated by the Brunauer-Emmett-Teller (BET) approach.

3. Results and discussion

3.1. Synthesis of highly ordered TM-doped mesoporous TiO₂

Fig. 1 presents the designed schematic way for the chelating-assisted soft-templating procedure to fabricate highly ordered mesoporous TM-doped TiO₂ (TM/OMT). Firstly, the pluronic F127 was applied as a structural-directing agent, the acetic acid as a chelating agent, and the metals nitrate salts, TOBT as metal and Ti precursor, respectively (the details are presented in Supplementary Table S1). The F127 surfactant co-assembles with the acetic acid-stabilized Ti precursor to form a composite through the evaporation process. Subsequently, the hydrophilic PEO segments of F127 with associated metal salts precursor were co-assembled into rod-like micelles in an ethanolic medium. After solidification by treating at 100°C for 24 h, the subsequent composite materials were rubbed and crushed into a powder form, which was then treated under annealing process at 350 °C in N₂ for 3 h, and 400 °C in the air for 3 h.

The photographs in Fig. 2a show a sequence of TM-doped OMT materials with dissimilar colors that could be obtained by altering the molar ratio of transition metals salt to titanium source through the self-assembly template process. As can be seen their a substantial color changes in the pure OMT caused by metal doping. The TM-doped OMT materials exhibit different colors for each dopant: brownish color for Mn/OMT, brownish-yellow for Fe/OMT, and yellow for Ni/OMT materials. Fig. 2b displays the absorption spectra of the bare-OMT and TM-doped OMT samples. The equivalent Tauc plots of the obtained materials and their band gaps are presented in Fig. 2c and Table 1, demonstrating that the band gaps of the TM-doped OMT can be tailored by varying of TM/Ti molar ratio. The assessed energy bandgap of the bare and doped OMT materials with various transition metals of Fe, Mn, and Ni are 2.59, 2.43, and 2.80 eV, correspondingly. The energy bandgap is witnessed to reduction with a TM-doping. It is worthy to note that the materials' bandgap is definitely tuned to an exact level to choose different TM-ions into host OMT materials; thus, red-shifting of optical absorption edge from UV to the visible region is witnessed. Obviously, the bare OMT materials exhibit a sharp absorbance at 400 nm, which can be assigned to the electronic transition from the valence band (VB) to the CB, corresponding to the bandgap (~3.09 eV) of bare OMT. However, the transition metal doping over OMT materials makes absorption above a wider range of the visible-light area with the broad absorption maxima at about 500 nm (Fe-OMT), 550 nm (Mn-OMT), and 480 nm (Ni-OMT). The enhancement in the absorption owing to the positive shift in the CB edge validates the TM-doped OMT's reduced bandgap and, thereby, a red-shift in light absorption (Liu et al., 2018).

Moreover, energy-dispersive X-ray spectroscopy (EDX) mapping was applied to examine the controllability and elemental dispersion of the TM dopant profile, as presented in Fig. 2(d,e,f). The TM-doping percentages in the fabricated materials were evaluated by EDX spectroscopy measurements (Fig. S1). The EDX mapping of TM-doped OMT samples shows the even distribution of the elements of Ti, Fe, Mn, and Ni on the OMT materials, exhibiting the uniform deposition of the TM dopants on the OMT framework.

The surface morphologies, lattice spacing, and porous structure of TM-doped OMT samples were directly observed by TEM and HRTEM analysis, and the results are presented in Fig. 3. The low magnification TEM images show that all the TM-doped OMT samples tend to have a highly-ordered mesoporous structure by possessing a pore size of (2–2.7 nm) and an identical shape to the undoped OMT (Fig. 3 a,b). All the TM-doped OMT materials display the uniform arrangement of nanostructured particles with its fine

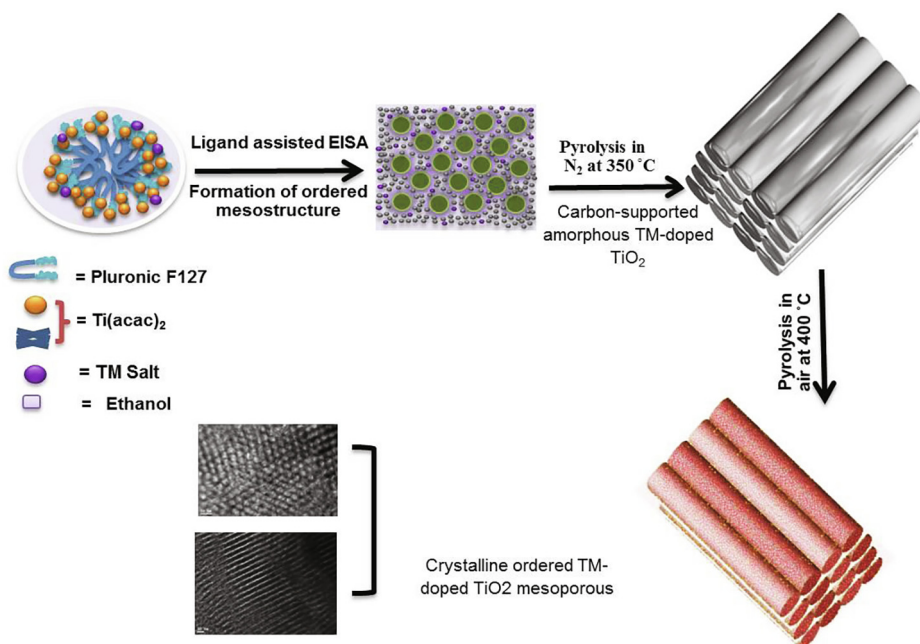


Fig. 1. Schematic representation of the formation process for chelating-assisted soft-template fabrication of highly ordered TM-doped mesoporous TiO_2 .

crystalline areas. Further, the uniform fringes can be evidently witnessed in the photographs of Fig. 3(a-e) agreeing to the bare and TM-doped OMT materials, which look like that the OMT materials exhibited highly crystalline in nature. The degree of crystallinity of the obtained anatase phase matches the premier intensity peak noticed in the diffraction pattern. The lattice fringe spacings were assessed to be (0.29, 0.32, and 0.35) agreeing to (001), (100), and (101) planes of anatase TiO_2 , respectively (Nguyen et al., 2011). The HRTEM images show that all the TM-doped TiO_2 (Fig. 3c-e) are crystalline with the same lattice fringe spacing as the pure anatase OMT, suggesting that the lattice of OMT doesn't change after TM doping. The crystallinity of the Fe-OMT materials was examined by pattern and depicted in Fig. 3f. The ring pattern observed in HR-TEM approves polycrystalline anatase features of TM-doped materials with brighter spots demonstrating the greater crystallinity of the Fe-doped-OMT with (101) plane. The SAED pattern recorded on the shell displays well-definite diffraction rings and spots (Fig. 3f inset), further confirming a crystalline anatase shell.

In order to further confirm the influence of the doped amount of TM on the crystalline features of TiO_2 was studied by XRD and N_2 sorption isotherms. The XRD spectra of TM-doped OMT samples are displayed in Fig. 4. The obtained diffraction patterns evidenced that the TM (Fe, Mn and Ni) doped OMT samples have a greatly crystalline anatase TiO_2 phase (JCPDS card No. 01-086-1157; Space group I41/amd) and have peaks that are identical to those of pure anatase OMT materials and have no distinct metal or metal oxide on the OMT surface. The assessed crystallite sizes of the OMT, Fe-OMT, Mn-OMT, and Ni-OMT samples are 6.97, 6.59, 7.16, and 6.80 nm corresponding to the XRD patterns shown in Fig. 4a, respectively. These results suggest that a homogeneous dispersion of metal dopants without varying the crystalline features of TiO_2 . The enlarged (101) diffraction peak of the pure TiO_2 , TM doped/OMT materials indicates no shift in 2θ values, and the (101) diffraction feature in all the OMT materials is evidenced to be strongly specifying the major crystal growth beside the same plane of anatase TiO_2 (Roy et al., 2013) (Fig. 4b). Also, there are no additional specific peaks of phases observed in the TM-doped samples,

evidencing no existence of doping-related elements like metal oxides. Thus, the nonexistence of any additional peaks in XRD patterns reveals the occupancy of TMs to the major sites of the TiO_2 lattice.

The textural features of obtained OMT and TM-OMT materials were examined by the N_2 -physisorption method (Fig. 5a, b). The N_2 sorption isotherm of all the OMT samples reveals distinguishing type-IV curves and H1 hysteresis loops with capillary condensation steps, typical of the mesoporous materials agreeing with IUPAC classification (Kruk and Jaroniec, 2001). According to the TEM analysis shown in Fig. 5a, the discrete capillary condensation at $P/P_0 = 0.4-0.8$ signifies the existence of cylindrical mesoporous pores. The OMT and TM-OMT samples' PSD was estimated from the adsorption data using the BJH method (Fig. 5b). Furthermore, the textural parameters, namely specific surface area, mesopore volume, and size of OMT, TM-OMT, and Co-OMT materials gotten from the N_2 sorption isotherms and BJH method (Fig. 5b) are shown in Table 1. All the TM/OMT samples had exceptional textural features with a specific surface area (218–260 $\text{m}^2 \text{g}^{-1}$ for TM-OMT), big pore volume (0.2–0.35 $\text{cm}^3 \text{g}^{-1}$), and uniform pore size (2–2.7 nm). The introduction of transition metals into the OMT leads to a reduction in the surface area. In contrast, compared with pure OMT, the surface area of TM-OMT materials was improved with the introduction of transition metals.

The amounts of TMs in the fabricated TM-OMT materials are evaluated through ICP. As listed in Table S2, the contents of metal oxides ranging from 0.0413 to 0.058. The XPS spectra analysis of TM-OMT samples was also performed to further ascertain TM's doping into OMT and their oxidation states (Li and Zeng, 2007) XPS survey spectrum of the fabricated TM-doped samples are presented in Fig. S2. The XPD fine Ti 2p of pure OMT, TM-OMT samples are shown in Fig. 6a. The Ti $2p_{3/2}$ and $2p_{1/2}$ photoelectron peaks of pure OMT are symmetric and their binding energy (BE) situations are at 459.53 eV and 465.28 eV, correspondingly suggesting the Ti^{4+} state (Tian et al., 2012). The spin-orbit splitting energy of the observed two peaks estimated to be 5.74 eV, identical to the literature value (Tian et al., 2012). As the metal is doped into OMT, the Ti $2p_{3/2}$ peaks of Ti in TM-OMT samples are also similar with

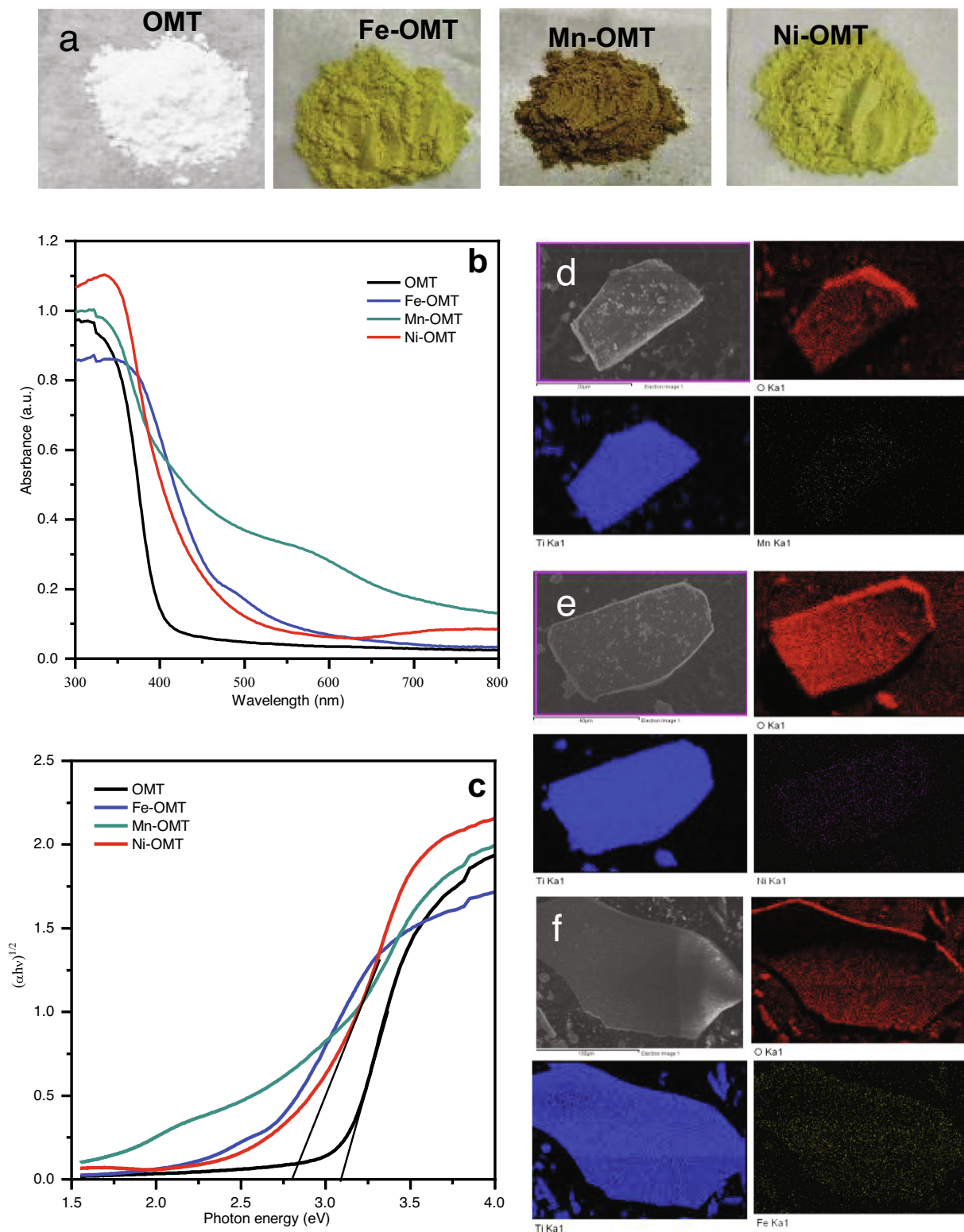


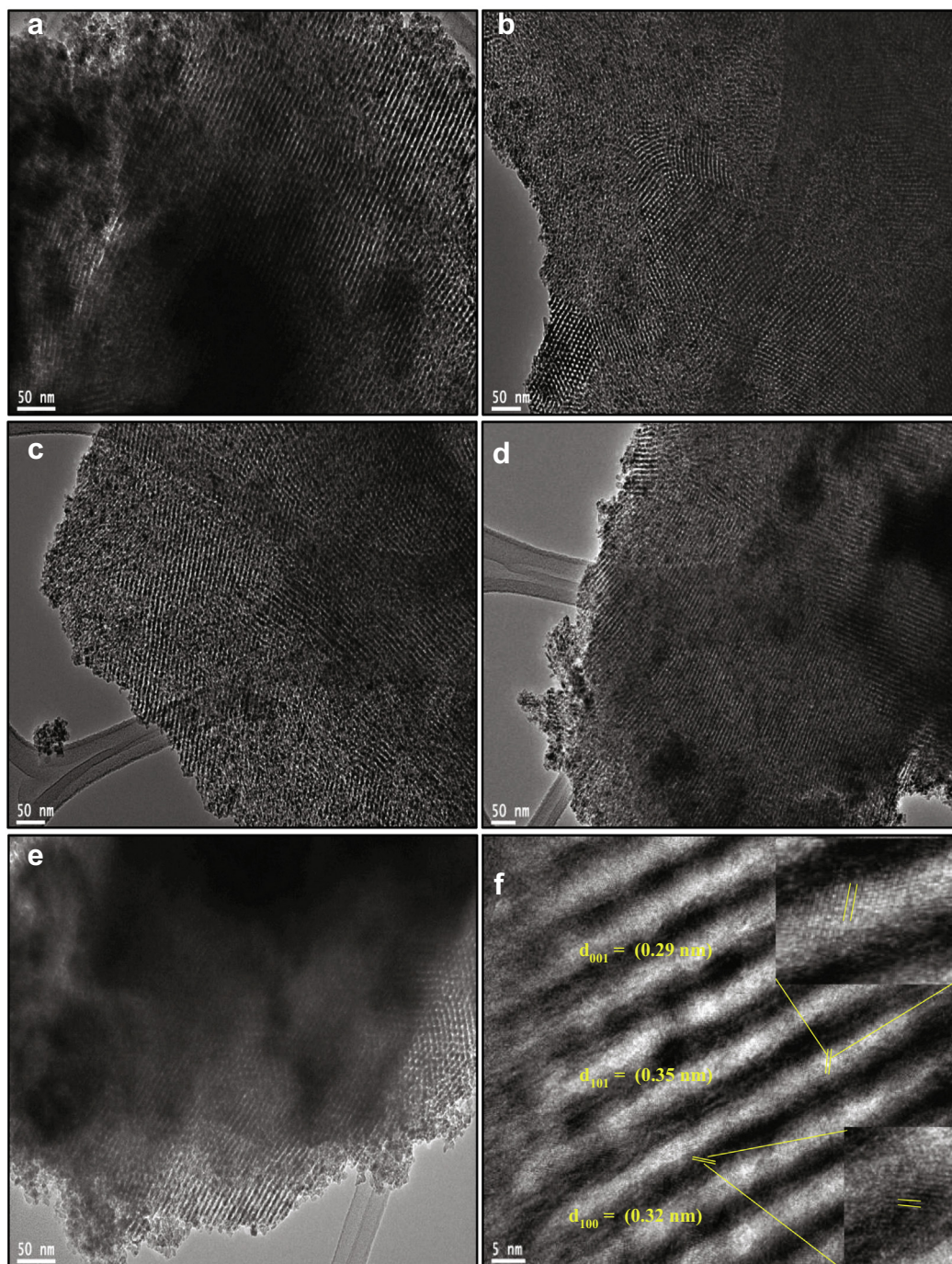
Fig. 2. Photographs are showing the color changes of OMT upon 4% molar ratio (M/Ti) Mn, Fe, and Ni doping (a) UV–visible absorbance spectra of TM-doped OMT. (b) and (c) its corresponding tauc plots, elemental EDAX mapping images of Mn/OMT (d), Ni-OMT (e), and Fe-OMT (f) materials prepared by self-assembly template route.

the pure except a slight red-shifted in the BE by 0.15 eV, for Fe, 0.1 eV, and 0, for Mn and Ni, respectively, signifying the substitution of Ti (iv) by TMs dopants (Duan et al., 2012). The shifting in BE values indicates that the Mn and Ni dopants' electron donation occurs significantly from Fe, probably due to the electron cloud's

movement toward electronegativity TMs. Fig. 6(b-e) displays XPS spectra of O1s region of pure OMT and TM-OMT samples. Fig. 6c displays that the O 1s of pure OMT show two dissimilar features of oxygen. Further, two fitted Gaussians peaks allotted as (1) and (2) were applied to fit the experimental data. The first peak (1) is

Table 1Textural parameters of pure of TiO₂ mesoporous and 4 wt% of different TM doped ordered mesoporous TiO₂ materials.

| Samples | Crystal phase | XRD Crystallite (grain) Size | S _{BET} (m ² /g) | Pore volume (cm ³ /g) | Pore size (nm) | Band gap eV |
|---------|--------------------------|------------------------------|--------------------------------------|----------------------------------|----------------|-------------|
| OMT | Anatase/TiO ₂ | 6.97 | 218 | 0.33 | 2.65 | 3.09 |
| Fe-OMT | Anatase/TiO ₂ | 6.59 | 260 | 0.35 | 2.44 | 2.59 |
| Mn-OMT | Anatase/TiO ₂ | 7.16 | 249 | 0.25 | 2.12 | 2.43 |
| Ni-OMT | Anatase/TiO ₂ | 6.80 | 259 | 0.30 | 2.67 | 2.80 |

**Fig. 3.** TEM images of (a, b) OMT, (c) Fe-OMT, (d) Ni-OMT, (e) Mn-OMT, (f) High-resolution TEM image of Fe-OMT.

observed at the lower BE of 530.7 eV, and is allotted to lattice oxygen of oxide of the TiO₂. The other peak (2) centered at 532.2 eV is correlated to the OH group adsorbed onto the OMT

materials' surface. However, The O 1s region of TM-OMT samples can be fitted into three Gaussian peaks labeled as (1), (2), and (3), (Fig. 6(b-e)). The peak situated at 530.7 eV fits to the Ti–O bonding

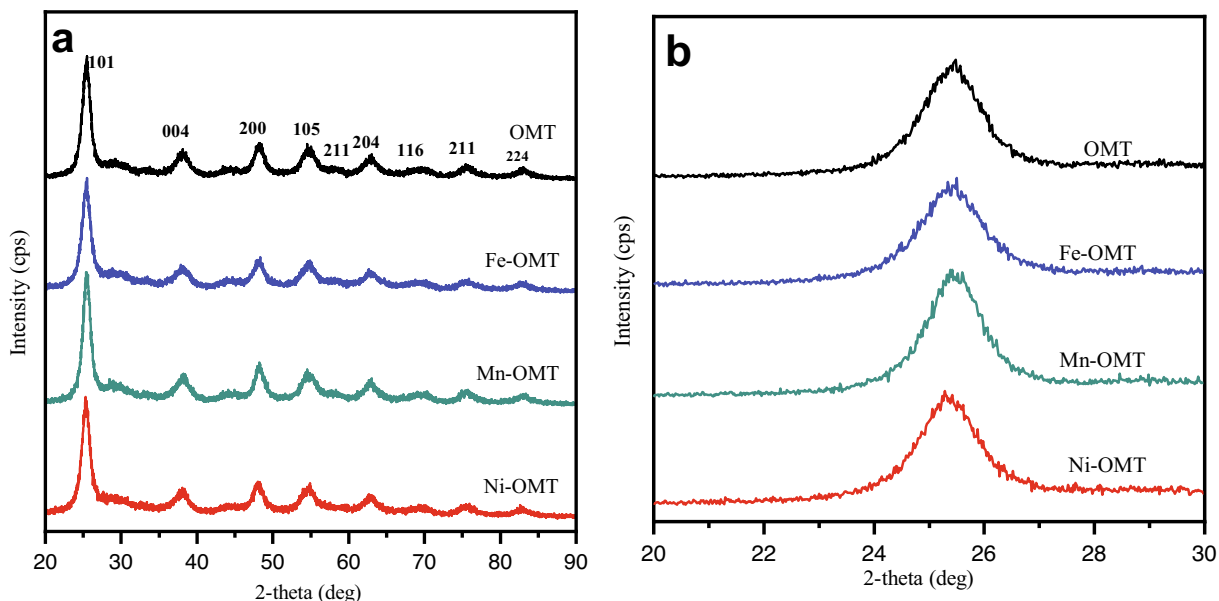


Fig. 4. (a) Wide-angle XRD pattern of the pure OMT and TM-OMT samples, (b) The enlarged (101) diffraction peak of the pure OMT, and TM-OMT samples.

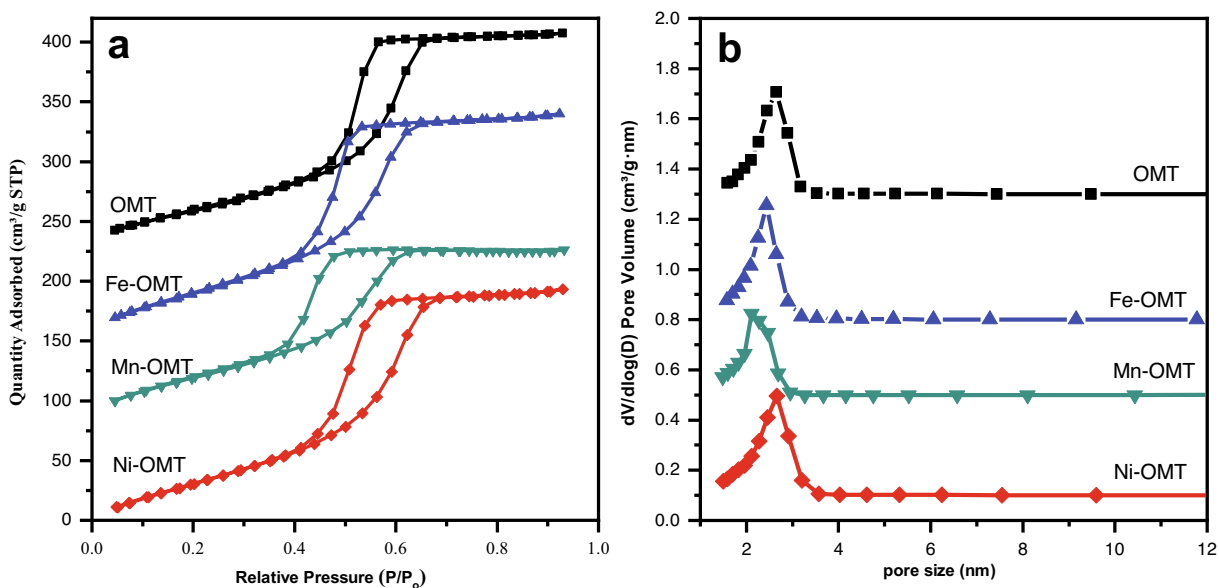


Fig. 5. (a) N_2 adsorption-desorption isotherms (b) BJH pore size distributions of pure OMT, and different transition metal-doped OMT samples prepared from self-assembly template route.

in TiO_2 . Peaks observed at 532.3 and 535.8 eV can be credited to the Ti-OH bonding and to the existence of adsorbed water. These examinations illustrated that TM dopants' loading in OMT materials generates an improved amount of surface oxygen vacancies in the nature of metal-OH bonds.

4. Conclusions

The soft-templating method was employed to fabricate different TM-doped ordered mesoporous TiO_2 materials and its physico-chemical properties were discussed in detail. The diffraction peak at $2\theta = 25.4^\circ$ in the XRD spectrum specifies that TM/OMT reveals

a pure anatase crystalline phase. The influence of TM doping level in OMT materials in the structural and morphological features was examined. The TM-doped OMT materials show that OMT substrates' formation is successfully modified with transition metal oxide particles. The optical examination of TM/doped OMT materials validates that the bandgap can be definitely modified with the types of transitional metal-ions into mesoporous TiO_2 . Particularly, the present in-situ EISA dopant approaches permit or homogeneous transition metals dopant dispersion with greater surface-active sites. This work opens a way to develop different transition metals loaded over highly ordered mesoporous TiO_2 substrate for various renewable energy production applications.

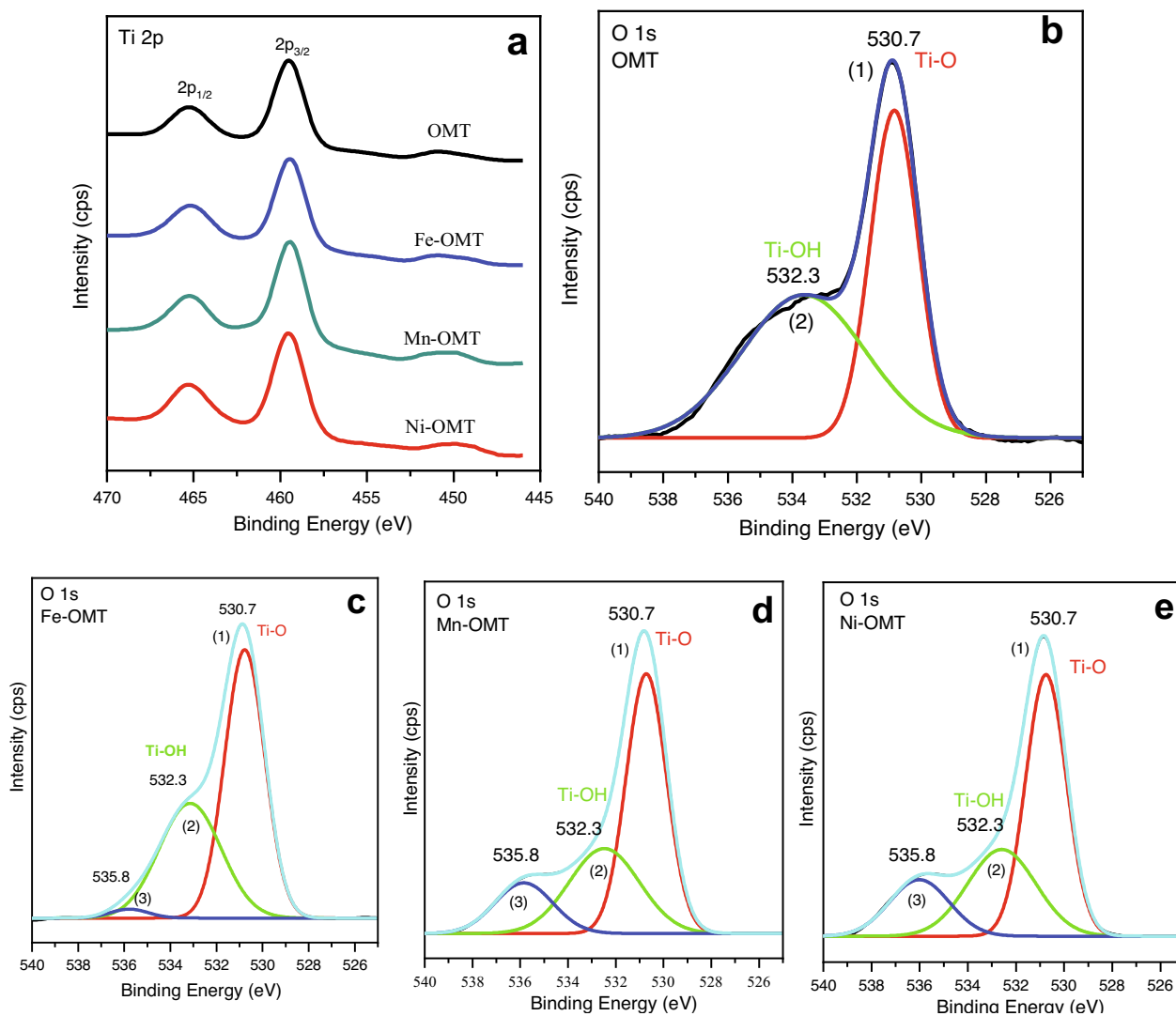


Fig. 6. Surface features of OMT and TM doped OMT samples. (a) Ti 2p XPS region spectra of pure OMT and different TM-doped OMT. O 1s region spectra of pure OMT (b), Fe-OMT (c), Mn-OMT (d), and Ni-OMT (e) prepared by self-assemble template route.

Funding

No funding was received for this work.

Declaration of competing interests

The authors declare that they have no known competing financial interests or personal relationships that could have appeared to influence the work reported in this paper.

Appendix A. Supplementary data

Supplementary data to this article can be found online at <https://doi.org/10.1016/j.jksus.2021.101469>.

References

Ahmad, M.S., Pandey, A.K., Abd Rahim, N., 2017. Advancements in the development of TiO₂ photoanodes and its fabrication methods for dye sensitized solar cell (DSSC) applications. *A review. Renew. Sustain. Energy Rev.* 77, 89–108.

- Antonelli, D.M., Ying, J.Y., 1995. Synthesis of hexagonally packed mesoporous TiO₂ by a modified sol-gel method. *Angewandte Chemie International Edition in English* 34, 2014–2017.
- Calleja, G., Serrano, D.P., Sanz, R., Pizarro, P., García, A., 2004. Study on the synthesis of high-surface-area mesoporous TiO₂ in the presence of nonionic surfactants. *Ind. Eng. Chem. Res.* 43, 2485–2492.
- Chung, C.C., Lee, C.S., Jokar, E., Kim, J.H., Diao, E.W.G., 2016. Well-organized mesoporous TiO₂ photoanode by using amphiphilic graft copolymer for efficient perovskite solar cells. *J. Phys. Chem. C* 120, 9619–9627.
- Duan, Y., Fu, N., Liu, Q., Fang, Y., Zhou, X., Zhang, J., Lin, Y., 2012. Sn-doped TiO₂ photoanode for dye-sensitized solar cells. *J. Phys. Chem. C* 116, 8888–8893.
- Even, J., Pedesseau, L., Jancu, J.M., Katan, C., 2013. Importance of spin-orbit coupling in hybrid organic/inorganic perovskites for photovoltaic applications. *J. Phys. Chem. Lett.* 4, 2999–3005.
- Fujishima, A., Honda, K., 1972. Electrochemical photolysis of water at a semiconductor electrode. *Nature* 238, 37–38.
- Fujishima, A., Rao, T.N., Tryk, D.A., 2000. Titanium dioxide photocatalysis. *J. Photochem. Photobiol., C* 1, 1–21.
- Jo, C., Hwang, J., Song, H., Dao, A.H., Kim, Y.T., Lee, S.H., Lee, J., 2013. Block-copolymer-assisted one-pot synthesis of ordered mesoporous WO₃-x/carbon nanocomposites as high-rate-performance electrodes for pseudocapacitors. *Adv. Funct. Mater.* 23, 3747–3754.
- Khojasteh, H., Salavati-Niasari, M., Mortazavi-Derazkola, S., 2016. Synthesis, characterization and photocatalytic properties of nickel-doped TiO₂ and nickel titanate nanoparticles. *J. Mater. Sci.: Mater. Electron.* 27, 3599–3607.
- Kruk, M., Jaroniec, M., 2001. Gas adsorption characterization of ordered organic-inorganic nanocomposite materials. *Chem. Mater.* 13, 3169–3183.

- Li, J., Zeng, H.C., 2007. Hollowing Sn-doped TiO₂ nanospheres via Ostwald ripening. *J. Am. Chem. Soc.* 129, 15839–15847.
- Li, L., Liu, C.Y., 2010. Mesoporous titania (A) nanoparticles prepared by a solvothermally treated organic small molecule system: formation mechanism and behavior in photocatalysis and dye-sensitized solar cells. *J. Phys. Chem. C* 114, 1444–1450.
- Li, Z., Haidry, A.A., Gao, B., Wang, T., Yao, Z., 2017. The effect of Co-doping on the humidity sensing properties of ordered mesoporous TiO₂. *Appl. Surf. Sci.* 412, 638–647.
- Liu, J., Duan, Y., Zhou, X., Lin, Y., 2013. Influence of VB group doped TiO₂ on photovoltaic performance of dye-sensitized solar cells. *Appl. Surf. Sci.* 277, 231–236.
- Liu, J., Li, Y., Ke, J., Wang, S., Wang, L., Xiao, H., 2018. Black NiO-TiO₂ nanorods for solar photocatalysis: Recognition of electronic structure and reaction mechanism. *Appl. Catal. B Environ.* 224, 705–714.
- Nguyen, C.K., Cha, H.G., Kang, Y.S., 2011. Axis-oriented, anatase TiO₂ single crystals with dominant 001 and 100 facets. *Cryst. Growth Des.* 11, 3947–3953.
- Nozik, A.J., 2002. Quantum dot solar cells. *Physica E: Low-dimensional Systems and Nanostructures* 14, 115–120.
- Reda, S.M., Khairy, M., Mousa, M.A., 2020. Photocatalytic activity of nitrogen and copper doped TiO₂ nanoparticles prepared by microwave-assisted sol-gel process. *Arabian J. Chem.* 13, 86–95.
- Roy, N., Sohn, Y., Pradhan, D., 2013. Synergy of low-energy 101 and high-energy 001 TiO₂ crystal facets for enhanced photocatalysis. *ACS Nano* 7, 2532–2540.
- Tian, F., Zhang, Y., Zhang, J., Pan, C., 2012. Raman spectroscopy: a new approach to measure the percentage of anatase TiO₂ exposed (001) facets. *J. Phys. Chem. C* 116, 7515–7519.
- Wagner, T., Haffer, S., Weinberger, C., Klaus, D., Tiemann, M., 2013. Mesoporous materials as gas sensors. *Chem. Soc. Rev.* 42, 4036–4053.
- Wang, H., Miao, J.J., Zhu, J.M., Ma, H.M., Zhu, J.J., Chen, H.Y., 2004. Mesoporous spherical aggregates of anatase nanocrystals with wormhole-like framework structures: their chemical fabrication, characterization, and photocatalytic performance. *Langmuir* 20, 11738–11747.
- Wang, T., Meng, X., Liu, G., Chang, K., Li, P., Kang, Q., Ye, J., 2015. In situ synthesis of ordered mesoporous Co-doped TiO₂ and its enhanced photocatalytic activity and selectivity for the reduction of CO₂. *J. Mater. Chem. A* 3, 9491–9501.
- Xie, Y., Huang, N., You, S., Liu, Y., Sebo, B., Liang, L., Zhao, X.Z., 2013. Improved performance of dye-sensitized solar cells by trace amount Cr-doped TiO₂ photoelectrodes. *J. Power Sources* 224, 168–173.
- Yu, J., Zhang, L., Cheng, B., Su, Y., 2007. Hydrothermal preparation and photocatalytic activity of hierarchically sponge-like macro-/mesoporous titania. *J. Phys. Chem. C* 111, 10582–10589.
- Zukalova, M., Zukal, A., Kavan, L., Nazeeruddin, M.K., Liska, P., Grätzel, M., 2005. Organized mesoporous TiO₂ films exhibiting greatly enhanced performance in dye-sensitized solar cells. *Nano Lett.* 5, 1789–1792.